Phys Chem Minerals (2004) 31: 313–320
DOI 10.1007/s00269-004-0389-8

ORIGINAL PAPER

A. Jones · M. S. Islam · M. Mortimer · D. Palmer

Alkali ion migration in albite and K-feldspar

Received: 18 June 2003/Accepted: 3 February 2004

Abstract As part of a study of ion migration mechanisms in feldspars, the dynamical behaviour of the alkali metal cations ions in albite and K-feldspar has been investigated using a combination of dielectric spectroscopy and atomistic computer simulation techniques. The low-frequency dielectric properties of these minerals have been studied from room temperature to 1100 K. At each temperature, the dielectric constant, conductivity and dielectric loss were determined over a range of frequencies from 100 Hz to 10 MHz. At high temperatures a distinct Debye-type relaxation in the dielectric loss spectra was observed for both albite and K-feldspar; the activation energy for these processes was determined to be 1.33 eV in both albite and K–feldspar. Atomistic simulation techniques were used to elucidate the mechanism and energetics of the cation migration processes. Mechanisms involving the conventional hopping of Na^+ and K^+ ions between cation sites in the (010) plane were found to give calculated energy barriers in good agreement with the experimentally determined activation energies. These results assist in understanding the nature of the processes responsible for the observed dielectric behaviour.

Keywords Albite · K-feldspar · Dielectric spectroscopy · Computer modelling · Ionic mobility

A. Jones (✉) · D. Palmer
Department of Earth Sciences,
The Open University, Walton Hall,
Milton Keynes, MK7 6AA, UK
e-mail: Alison.a.jones@btinternet.com
Tel.: 0044 1234 364315

M. S. Islam
Department of Chemistry,
University of Surrey, Guildford GU2 5XH, UK

M. Mortimer
Department of Chemistry,
The Open University, Walton Hall,
Milton Keynes, MK7 6AA, UK

Introduction

The feldspar minerals consist of end-member phases albite, $NaAlSi_3O_8$, K-feldspar, $KALSi_3O_8$, and anorthite, $CaAl_2Si_2O_8$, and they are the most commonly occurring minerals in the Earth's crust. Diffusion of alkali ions in feldspars is of geological interest as it determines the rates of alkali ion exchange between alkali feldspars and their surroundings, and of exsolution. This process is also of interest because of its connection with the diffusion of trace elements, including argon, into or out of alkali feldspar crystals (Wartho et al. 1999; Fulda and Lippolt 2000). There is an abundance of data describing the bulk diffusion of cations in feldspars and related minerals (Bailey 1971; Lin and Yund 1972; Yund 1983; Giletti and Shanahan 1997) and there is some evidence from measurements of diffusion coefficients that alkali diffusion in feldspars occurs more readily in the (010) plane (Petrovic 1972; Giletti et al. 1974). However, there is a paucity of published data regarding the atomic mechanisms of these diffusion processes. Rates of diffusion on a macroscopic scale are inherently dependent on microscopic controlling factors and these can only be established by investigating the mechanisms and energetics of ion migration on an atomic scale.

The feldspar minerals comprise an aluminosilicate framework of corner sharing Si- and Al-tetrahedra with a range of cations in large structural cavities. A study carried out on the coordination of Na and K atoms in low albite and microcline (Downs et al. 1996) has suggested that strong interactions exist between mobile species, such as alkali cations, and the surrounding framework. An investigation which establishes a more precise picture of ionic mobility, at a microscopic level, should provide an insight into the intrinsic constraints controlling the mechanisms of ion diffusion in these minerals.

Ionic transport in crystalline solids may occur by a process of activated hopping between occupied and vacant sites or by a correlated motion of ions along a channel. Short-range mobilities can be described by an

activated-hopping model (Debye 1929; Ohgushi and Kazuhide 1998), whereas longer-range mobility in channel structures is more likely to occur by a correlated motion of ions along a channel (Barrer and Saxon-Napier 1962; Alpen et al. 1977). Although there are no clearly defined diffusion pathways within the feldspar structure, there is some evidence that alkali feldspars exhibit anisotropy of diffusion. Petrovic (1974) pointed out that possible interstitial sites and large cation vacancies are connected only in the (010) plane and that alkali diffusion is most likely to occur by a vacancy mechanism.

Cation migration within the albite and K-feldspar structures has been investigated using an approach developed for a successful study of nepheline (Jones et al. 2001) in which a combination of dielectric spectroscopy and computer modelling techniques were used to determine the most likely migration pathway for Na^+ ions in nepheline. Low-frequency dielectric spectroscopy provides a structural probe for measuring the behaviour of loosely bound channel ions in framework minerals, as only the mobile charged species respond to the relatively low frequency (<10 MHz) electric fields. In the present study, dielectric spectroscopy is used to investigate the mobility of Na^+ ions in albite and K^+ ions in K-feldspar from room temperature to 1100 K. Atomistic lattice simulations have been used to probe possible diffusion pathways and thereby provide an insight into the energetics and mechanisms of the ion migration processes observed using dielectric spectroscopy. The simulation methods are well established and similar studies have been used to investigate ion transport in various inorganic solids (Catlow 1992a; De Souza et al. 1999; Fisher and Islam 1999; Islam 2000).

Methods

The materials used in this study were a sample of albite originating from Brazil and a K-feldspar, BM1924,1244 (origin unknown) from the Natural History Museum. The samples used for the dielectric spectroscopy measurements were cut from large crystals and were free from cracks. The compositions of the albite and K-feldspar samples, as determined by electron microprobe analysis, were $Na_{0.99}Al_{1.01}Si_{2.98}O_8$ and $Na_{0.08}K_{0.92}Al_{1.02}Si_{2.98}O_8$, respectively.

Dielectric spectroscopy

The dielectric data were collected using an experimental arrangement similar to that used by Palmer and Salje (1990) and as described previously (Jones et al. 2001). Thin sections from selected crystals were cut and polished into smooth discs (ca. 5 mm diameter, 0.7 mm thick). Individual discs were placed between two platinum electrodes (diameter 3 mm) which were connected via shielded coaxial cable to a Hewlett Packard HP4192 A Impedance Analyser. Good electrical contact was maintained using a pyrophyllite block resting on the supported electrode sandwich. The assembly was mounted within a vertical tube furnace and a thermocouple positioned approximately 5 mm from the sample. The furnace, which was calibrated using the known phase-transition temperatures of sodium niobate (Darlington and Knight 1999), was estimated to be accurate to within ± 5 K. This arrangement enables capacitance (C) and conductance (G) to be measured over a range of temperatures as a function of the frequency of the applied electrical field. The computer-controlled Impedance Analyser provided logarithmic frequency sweeps from 100 Hz to 10 MHz (sampling 101 frequencies), recording mean values (averaged over 1 s) of C and G for each frequency. Background contributions due to instrumental effects were assumed to be temperature-independent and calculated as an additive constant from measurements made on a test shunt on the analyser and in the furnace at room temperature (Palmer and Salje 1990; Palmer 1995). Capacitance and conductance measurements were made at room temperature and then at regular intervals up to 1100 K. From these measurements the dielectric loss (tanδ) was calculated at each frequency. The dielectric loss is directly related to the real and imaginary parts of the dielectric permittivity, ε' and ε'' respectively. In an ac field with frequency ω it can be shown that:

$$\tan\delta = \frac{\varepsilon''}{\varepsilon'} = \frac{G}{C\omega}$$

Measurement of tanδ as a function of frequency of the applied field can be used as a measure of the energy absorbed by polarising species in a dielectric material. If the dielectric response of the material is measured as a function of frequency, it is found that there are regions of increased dielectric loss and sharp drops in the dielectric constant at certain frequencies, known as dispersion regions. The rate of energy transfer to the surroundings can be assumed to be an exponential process with a characteristic time constant τ, the relaxation time, which is determined by the strength of the interaction between the dipole and the system to which it is transferring energy. (If the period of oscillation of the applied field is less than τ, the dipole will not be able to follow the field.) These relaxations can be described using the Debye equations.

The fundamental assumption of Debye theory (Debye 1929) is that the dielectric relaxation follows an exponential function and that under a constant electric field, the sample polarisation, $P(t)$, increases with time at an exponential rate to a saturation value $P(\infty)$, the magnitude of which will depend on the applied field:

$$P(t) = P(\infty)[1 - \exp(-t/\tau)],$$

where τ, the time constant or relaxation time, defines the slowness of the induced polarisation increase. The Debye equations can be derived using this assumption:

$$\varepsilon' = \varepsilon_\infty + \frac{\varepsilon_s - \varepsilon_\infty}{1 + \omega^2\tau^2} \text{ and } \varepsilon'' = \frac{(\varepsilon_s - \varepsilon_\infty)\omega\tau}{1 + \omega^2\tau^2},$$

where ε_∞ is the permittivity at infinite frequency and ε_s is the permittivity for a static field.

As the movement of the position of the maximum in tan δ with temperature shows an Arrhenius-type temperature dependence, an activation energy for the relaxation process can be measured:

$$\tau = \tau_0 \exp\left(\frac{-E_a}{k_B T}\right),$$

where τ depends on the activation energy, E_a, the temperature, T, and the Boltzmann constant, k_B. These relations have been used to calculate the activation energies for the observed relaxation processes.

Atomistic computer modelling

The computational techniques used in this work, embodied in the GULP code (Gale 1997), are well established and have been reviewed in detail elsewhere (Catlow 1987). The calculations are based upon the Born model of a solid which includes a long-range Coulombic interaction between each pair of ions i and j, and a short-range Buckingham term to model overlap repulsions and van der Waals forces. The electronic polarisability of the ions is described by the shell model which has been found to be effective in simulating the dielectric and lattice dynamical properties of metal oxides (Catlow 1992b). For aluminosilicates, it is also necessary to include an angle-dependent term in the potential for O–Si–O or O–Al–O.

It should be stressed that employing such a potential model does not necessarily imply that the electron distribution corresponds to a fully ionic system. The validity of the model is assessed primarily by its ability to reproduce observed crystal properties, and it is found that models based on formal charges work well, even for compounds such as silicates and zeolites in which there is a significant degree of covalency (Catlow 1992b; Higgins et al. 2002; Sastre et al. 2002). Indeed, the nepheline structure has successfully been reproduced using this model (Jones et al. 2001).

The calculation of defect formation and migration energies utilised the two-region Mott–Littleton methodology for accurate modelling of defective lattices. An important feature of these calculations is the treatment of lattice relaxation about the point defect, or migrating ion, so that the crystal is not considered as a rigid lattice. The GULP code allows fractional occupancies to be specified for crystallographic sites by a mean field approach (Gale 1997). It was therefore possible to model the albite and K-feldspar structures (in which the ratio of Si:Al is 3:1), with a homogeneous distribution over the Si/Al sites. All defect calculations were carried out on a $2a2c$ supercell in which an isolated vacancy was created.

The interatomic potentials and shell model parameters used (listed in Table 1) were all taken from previous simulation studies (Freeman and Catlow 1990) where reliability in modelling silicates and aluminosilicates has been demonstrated widely (Catlow 1992b). They were also used in the recent simulation of the nepheline structure (Jones et al. 2001), where they gave excellent agreement with experimentally determined parameters.

The starting point for the present calculations was the simulation of the albite and K-feldspar structures. Structure refinements of compositions similar to those used in this study were selected for the assessment of the potential model: a fully disordered high albite structure, $NaAlSi_3O_8$, (Winter et al. 1979) and a K-feldspar (sanidine) structure, $Na_{0.1}K_{0.9}AlSi_3O_8$, (Phillips and Ribbe 1973) with a composition similar to that used in the present work. The unit-cell dimensions and atomic coordinates were equilibrated under constant pressure and the calculated values for the lattice parameters were compared with the experimental values (Table 2). Overall there is good agreement between the experimental and simulated structures for these complex systems. However, the a lattice parameter in K-feldspar shows the largest difference between the experimental and calculated values and this may reflect uncertainties in the K^+ defect distribution along this axis.

Table 1 Interatomic potentials used for modelling the feldspar structures

(a) Two-body Buckingham : $V_{ij}(r_{ij}) = A_{ij}\exp(-r/\rho_{ij}) - C/r_{ij}^6$

Interaction[a]	A/eV	ρ/Å	C/eV Å^{-6}
$Na^+...O^{2-}$	1226.84	0.3065	0.0000
$K^+...O^{2-}$	902.8	0.36198	0.0000
$Si^{4+}...O^{2-}$	1283.907	0.32052	10.66158
$Al^{3+}...O^{2-}$	1460.3	0.29912	0.0
$O^{2-}...O^{2-}$	22764.3	0.1490	27.879

(b) Shell model[b]

Species	Y/e	k/eV Å^{-2}
O^{2-}	−2.86902	74.92

(c) Three-body[c]: $V_{3\text{-body}} = (1/2)k(\theta - \theta_0)^2$

Interaction	Force constant/eV rad^{-1}	θ_0
O–Si–O	2.0972	108.693
O–Al–O	2.0972	109.470

[a] Potential cutoff = 10 Å
[b] Y and k refer to the shell charge and harmonic force constant, respectively
[c] θ_0 is the equilibrium bond angle

Table 2 Calculated and experimental structural parameters for the feldspars

(a) Albite

Parameter	Experimental	Calculated	Difference (%)
Unit-cell volume Å^3	770.2033	781.4753	1.46
a/Å	8.2970	8.4573	1.93
b/Å	12.9940	12.9664	−0.21
c/Å	7.1440	7.1263	−0.25
α/°	90.00	90.6229	0.69
β/°	116.01	116.17	0.13
γ/°	90.00	90.12	0.13

(b) K-feldspar

Parameter	Experimental	Calculated	Difference (%)
Unit-cell volume Å^3	797.8388	832.6996	4.36
a/Å	8.539(4)	8.9142	4.39
b/Å	13.015(5)	12.9886	−0.20
c/Å	7.179(3)	7.1919	0.18
α/°	90.00	90.00	0.00
β/°	115.99	115.81	−0.15
γ/°	90.00	90.00	0.00

Results and discussion

Dielectric spectroscopy

The temperature and frequency dependences of the dielectric constant, ε', and the dielectric loss, tan δ, for albite and K-feldspar between 900 and 1100 K are shown in Figs. 1 and 2, respectively. It can be seen that the patterns of behaviour for albite and K-feldspar are very similar. The dielectric constant has a value close to 8 for all frequencies at room temperature, rising slowly at low frequencies up to 800 K, after which there is a dramatic increase (the greatest changes being at low frequencies). No significant dielectric loss peak was observed below 900 K and there was no evidence of any low-frequency (below 5 kHz) absorption which would be indicative of large-scale motions such as bulk diffusion or ionic conduction (Barrer and Saxon–Napier 1962; Jones et al. 2001). The temperature dependence of the frequency of the maximum absorption for each mineral follows an Arrhenius relationship as shown in Fig. 3. The calculated activation energies are 1.33 ± 0.02 eV (128.3 ± 1.9 kJ mol^{-1}) and 1.33 ± 0.03 eV (128.4 ± 3.0 kJ mol^{-1}) for albite and K-feldspar, respectively.

Ion migration mechanisms and energetics

Albite

A possible migration pathway for a Na^+ ion in albite would be to follow a trajectory in the (010)

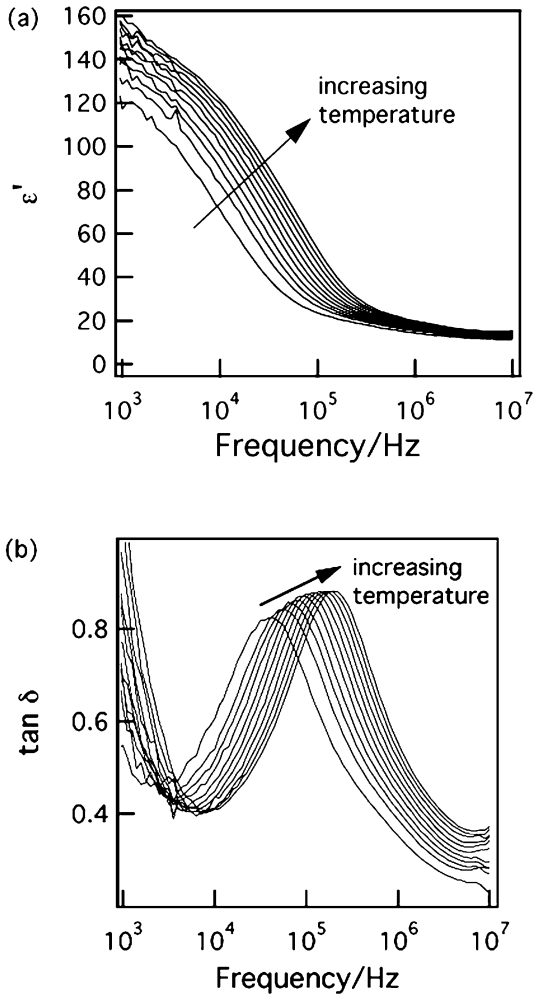

Fig. 1a,b Temperature and frequency dependence of **a** dielectric constant and **b** dielectric loss for albite between 963 and 1073 K

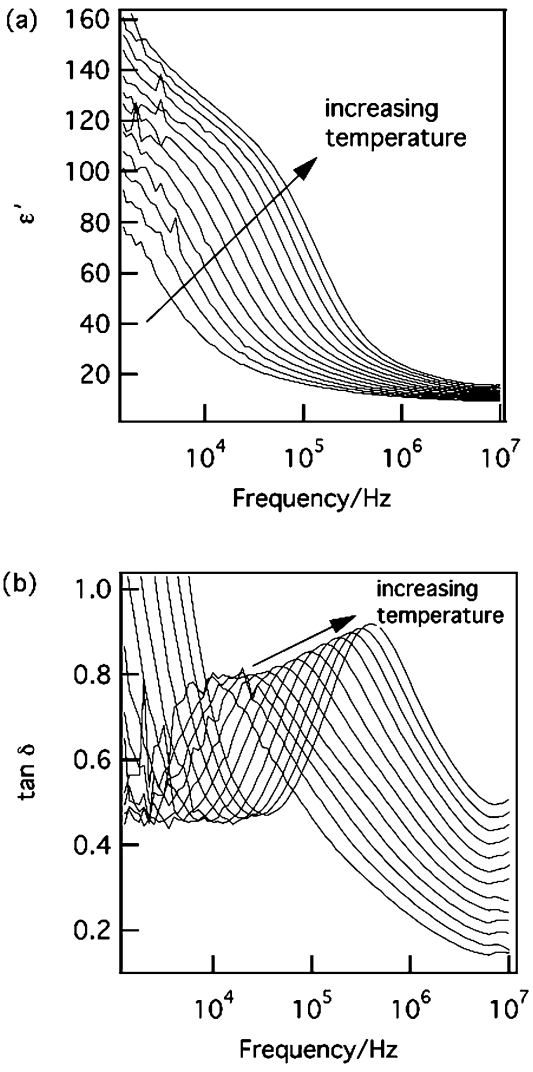

Fig. 2a,b Temperature and frequency dependence of **a** dielectric constant and **b** dielectric loss for K-feldspar between 902 and 1083 K

plane between an occupied and vacant Na^+ site, as shown in Fig. 4. In order to determine the approximate route taken by a migrating Na^+ ion between the two sites, lattice energy calculations were carried out across the (010) plane of translation. The results of these calculations suggested that the optimum migration route would be a linear pathway, as shown in Fig. 5. The migration energy of the Na^+ ion along this pathway was determined by calculating the defect energy at different points along the pathway, allowing full relaxation of the lattice at each point. In this way the saddlepoint configuration was identified from the energy profile (Fig. 6) and the energy barrier to migration was calculated. This was calculated to be 1.31 eV, which is in very good agreement with the activation energy determined from the dielectric measurements (1.33 ± 0.02 eV). This result suggests that the process being observed in the dielectric spectroscopy is due to the migration of Na^+ ions along a linear trajectory as described above and as shown in Fig. 5.

K-feldspar

The most likely migration pathway for a K^+ ion within the K-feldspar structure is along a linear trajectory, similar to that mapped out for albite, in the (010) plane. Such a pathway between an occupied and vacant site would offer the most energetically favourable route in terms of the proximity of the K^+ ion to the nearest-neighbour oxygens at the saddlepoint position. The calculated energy profile for K^+ ion migration along this pathway is shown in Fig. 7, and the energy barrier to migration is calculated to be 0.99 eV.

Other similar migration pathways in the (010) plane were also investigated. Two of these are shown, together with the pathway described above, in Fig. 8. They both yielded higher activation energies (listed in Table 3). This is probably due to the narrower bottleneck width (measured between the nearest oxygen atoms in the (010) plane at the saddlepoint).

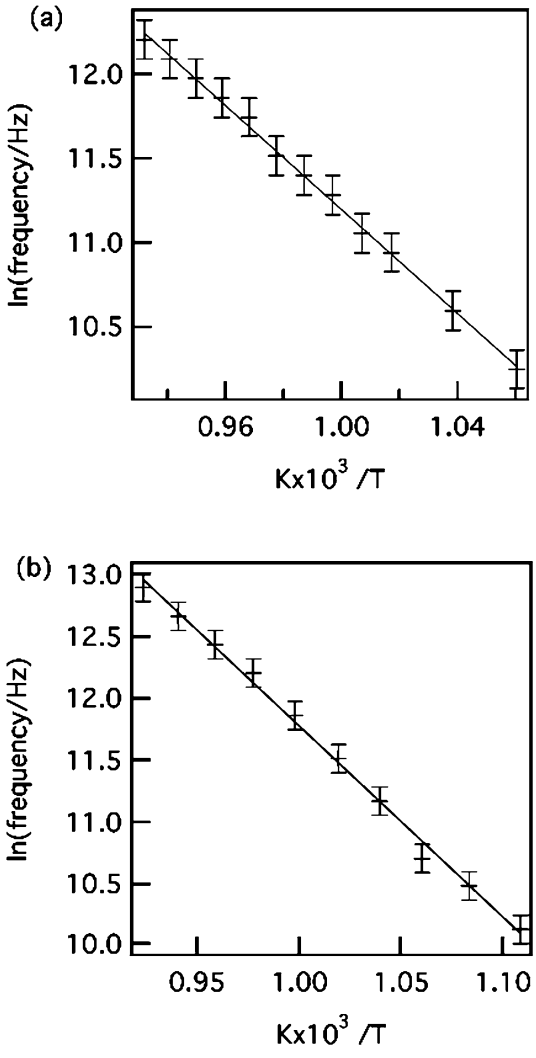

Fig. 3a,b Arrhenius plot showing the temperature dependence of the maxima in the dielectric loss for **a** albite and **b** K-feldspar. The *gradients of the lines* indicate activation energies of 1.33 ± 0.02 eV and 1.33 ± 0.03 eV, respectively. The *error bars* represent the uncertainty in determining the peak position at each temperature

Fig. 4 A view of part of the albite structure showing a path through an interconnecting channel between an occupied and a vacant Na^+ site in the (010) plane

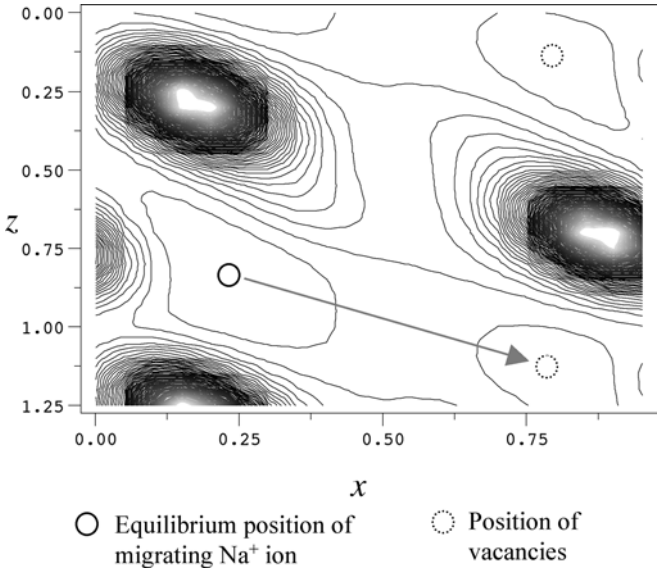

Fig. 5 Contour plot showing the variation in lattice energy in the (010) plane in albite. The migration pathway of a migrating Na^+ ion and vacant Na^+ sites are indicated

The activation energy determined from the dielectric spectroscopy measurements was 1.33 ± 0.03 eV. It can be seen from Table 3 that the activation energy is highly sensitive to the channel width. The discrepancy in the calculated structure could account for the difference between the calculated and experimentally determined activation energies for K-feldspar. In any case, of these values, the calculated energy of 0.99 eV is in general accord with the observed activation energy.

It is somewhat surprising to find that the experimentally determined activation energy for the migration of a small Na^+ ion in albite is almost identical to that found for the migration of the much larger K^+ ion in K-feldspar along a similar trajectory in the (010) plane. It can be seen from the lattice parameters given in Table 2 that K-feldspar has a more open structure than albite: both the calculated and the experimentally determined values of the *a* parameter are greater in K-feldspar. However, this fact alone cannot be used to explain the similarity in the experimentally-determined activation energies. Additional calculations were therefore carried out in order to investigate the effect of changing the

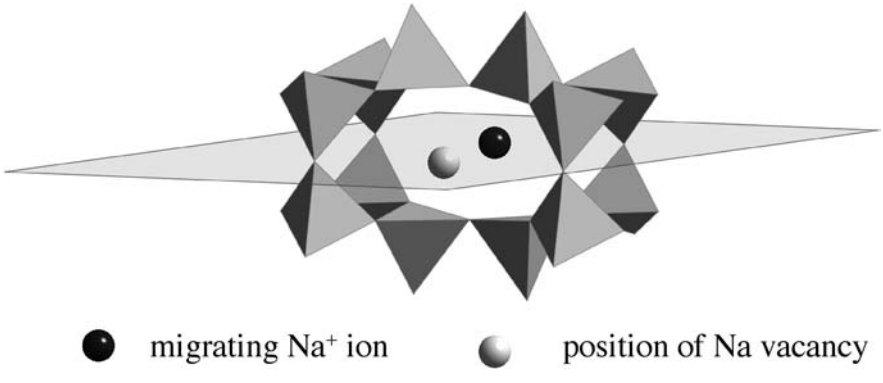

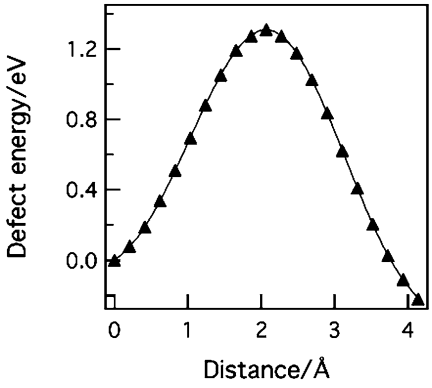

Fig. 6 The calculated energy profile for a Na^+ ion migrating from its equilibrium position to an adjacent vacancy in albite. The *points* indicate the calculated defect energies at locations along the linear migration pathway

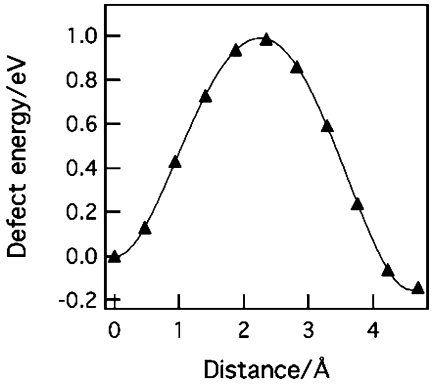

Fig. 7 The calculated energy profile for a K^+ ion migrating from its equilibrium position to an adjacent vacancy in K-feldspar. The *points* indicate the calculated defect energies at locations along the linear migration pathway

interstitial cation on the framework structures of both albite and K-feldspar.

An interstitial K^+ ion was inserted into the albite structure and the migration energy calculated for the same pathway as Na^+ ion migration in the (010) plane. Similarly, the migration energy of an interstitial Na^+ ion was calculated for the same trajectory, pathway (i), described for K^+ ion migration in K-feldspar. The results of these calculations are compared with those of the previously described defect calculations in Table 4.

The results indicate that the more open structure of K-feldspar facilitates a lower energy migration pathway for either cation compared to albite. They also provide supporting evidence that the processes observed in the dielectric spectroscopy data relate to Na^+ and K^+ ion migration in albite and K-feldspar, respectively. Although the unrelaxed bottleneck widths of the two structures differ, both structures relax around the migrating cation in order to accommodate it at the saddlepoint (Table 4). As an example illustration, Fig. 9 shows the relaxation around the K^+ ion at the saddlepoint in K-feldspar. It can be seen from Table 4 how the bottleneck in albite widens to allow the migration

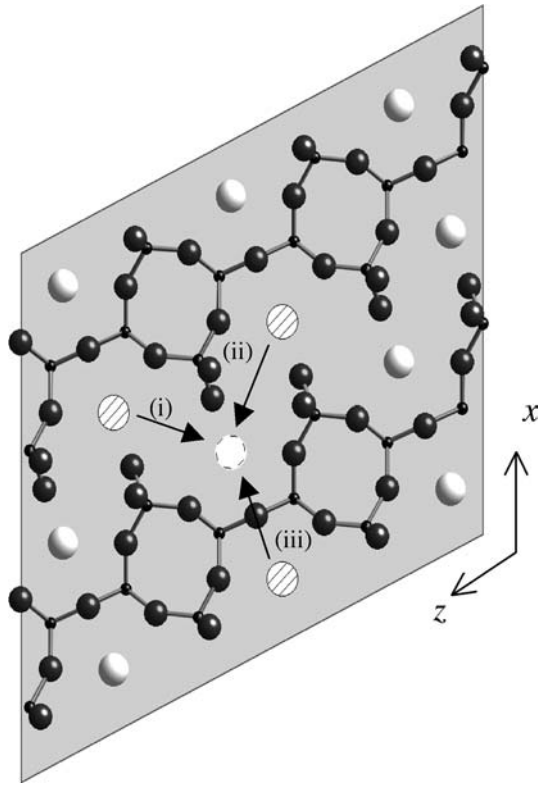

Fig. 8 View of the (010) migration plane in the K-feldspar structure showing three possible K^+ ion migration pathways (*i*), (*ii*) and (*iii*). The vacant site is shown as a *dashed open circle*

Table 3 Calculated energy barriers and bottleneck widths for the migration of K^+ in the (010) plane in K-feldspar

Channel[a]	Unrelaxed bottleneck width (Å)	Calculated energy barrier (eV)
(i)	5.47	0.99
(ii)	3.97	2.29
(iii)	3.88	2.92

[a] Fig. 8

Table 4 Calculated migration energies and bottleneck widths for interstitial Na^+ and K^+ ions in albite and K-feldspar

Interstitial ion at saddlepoint	Energy (eV)	Bottleneck width (Å)	
		Unrelaxed	Relaxed[a]
K^+ ion in albite	1.86	4.57	5.22
Na^+ ion in albite	1.31	4.57	4.70
K^+ ion in K-feldspar	0.99	5.47	5.65
Na^+ ion in K-feldspar	0.70	5.47	5.30

[a] Ion at saddlepoint

of Na^+ or K^+ ions; the corresponding channel in K-feldspar contracts around the smaller Na^+ ion when it is at the saddlepoint, but expands to allow the migration of larger K^+ ion through the same bottleneck.

The simulations illustrate how the feldspar framework responds to ion movement within the structure at

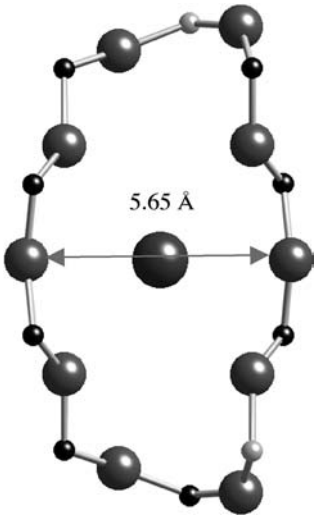

Fig. 9 Relaxation of the migration channel in K-feldspar with the migrating K^+ ion at the saddlepoint (viewed down [101])

the atomic level; this information is difficult to extract from experiment alone. Overall, it appears that the presence of vacancies and interstitial ions may have a significant effect on the dimensions of the interconnecting channels between the cation sites. Our simulations therefore indicate the importance of regarding ion migration as a process involving framework relaxation, rather than merely a static framework through which ions diffuse.

Conclusion

The combined dielectric spectroscopy and computer modelling approach presented here has provided a means of determining a mechanism for the experimentally observed ion-migration processes that occur in albite and K-feldspar. By taking into account the complexity of the structures and the variable response of the framework to changes in site occupancy, it has been possible to show how the energetics of ion-migration processes are influenced by framework geometry and ion size. In conclusion:

1. The migration of interstitial cations in the alkali feldspar structures occurs in the (010) plane. At high temperatures a distinct Debye-type relaxation in the dielectric loss spectra was observed for both albite and K-feldspar; the activation energy for these processes was determined to be 1.33 ± 0.02 eV in both albite and K-feldspar. Mechanisms involving the conventional hopping of Na^+ and K^+ ions between cation sites in the (010) plane were found to give calculated energy barriers in good agreement with the experimentally determined activation energies.
2. The most energetically favourable pathway for ion migration in the feldspars is a linear pathway between cation sites in the (010) plane. This is in contrast with earlier studies of Na diffusion in nepheline (Jones et al. 2001) in which it was found that a curved path between the occupied and vacant sites was the lowest energy pathway.
3. The local lattice relaxations derived from the computer simulations have shown how the presence of vacancies and interstitial ions can have a significant effect on the width of a bottleneck, and hence the energetics of cation-migration processes.

References

Alpen UV, Schulz H, Talay GH (1977) One-dimensional cooperative Li-diffusion in beta-eucryptite. Solid State Commun 23: 911–914

Bailey A (1971) Comparison of low-temperature with high-temperature diffusion of sodium in albite. Geochim Cosmochim Acta 35: 1073–1081

Barrer RM, Saxon-Napier EA (1962) Dielectric properties of basic sodalite and a silver nitrate–zeolite complex. Trans Faraday Soc 58: 145–155

Catlow CRA (1987) Computational techniques and simulation of crystal structures. Clarendon Press, Oxford

Catlow CRA (1992a) Can the mechanisms of ion transport in SSIs be determined by computer modelling. Solid State Ionics 53–56: 955–963

Catlow CRA, ed (1992b) Modelling of structure and reactivity in zeolites. Academic Press, London

Darlington CNW, Knight KS (1999) On the lattice parameters of sodium niobate at room temperature and above. Physica B: Condens Matter 266:(4) 368–372

De Souza R, Islam MS, Ivers-Tiffee E (1999) Formation and migration of cation defects in the perovskite oxide $LaMnO_3$. J Mat Chem 9: 1621–1627

Debye P (1929) Polar molecules. Chemical Catalogue Company, New York

Downs RT, Andalman A, Hudacsko M (1996) The coordination numbers of Na and K atoms in low albite and microcline as determined from a procrystal electron-density distribution. Am Mineral 81: 1344–1349

Fisher CAJ, Islam MS (1999) Defect, protons and conductivity in brownmillerite-structured $Ba_2In_2O_5$. Solid State Ionics 118: 355–363

Freeman CM, Catlow CRA (1990) A computer modelling study of defect and dopant states in SnO_2. J Solid State Chem 85: 65–75

Fulda C, Lippolt HJ (2000) Diffusion coefficients of noble gases in natural minerals: an apparent experimental time dependence caused by domain size spectra. Math Geol 32(1): 31–47

Gale JD (1997) GULP: a computer program for the symmetry adapted simulation. J Chem Soc, Faraday Trans 93:(4) 629–637

Giletti BJ, Semet MP, Kasper RB (1974) Self-diffusion of potassium in low albite using an ion microprobe. Geological Society of America Washington.DC Abstracts with Programs 6: 754

Giletti BJ, Shanahan TM (1997) Alkai diffusion in plagioclase feldspar. Chem Geol 139: 3–20

Higgins FM, de Leeuw NH, Parker SC (2002) Modelling the effect of water on cation exchange in zeolite A. J Mat Chem 12: 124–131

Islam MS (2000) Ionic transport in ABO_3 perovskite oxides: a computer modelling tour. J Mat Chem 10: 1027–1038

Jones A, Palmer D, Islam MS, Mortimer M (2001) Ion migration in nepheline: a dielectric spectroscopy and computer modelling study. Phys Chem Miner 28: 28–34

Lin TH, Yund RA (1972) Potassium and sodium self-diffusion in alkali feldspar. Contrib Min Petrol 34: 177–184

Ohgushi T, Kazuhide K (1998) Movements of sodium ions in mordenite and their assignment. J Chem Soc, Faraday Trans 94: 3769–3775

Palmer DC (1995) Dielectric spectroscopy: a novel way to measure ionic and molecular mobility in minerals. Terra Abstracts 7:(10) 80

Palmer DC, Salje EKH (1990) Phase transitions in leucite: dielectric properties and transition mechanism. Phys Chem Miner 17: 444–452

Petrovic R (1972) Alkali ion diffusion in alkali feldspars, PhD, Dissertation, Yale University, New Haven, Connecticut

Petrovic R (1974). Diffusion of alkali ions in alkali feldspars. In: The feldspars, McKenzie WS, Zussman J (eds) Manchester University Press, Manchester, pp 174–182

Phillips MW, Ribbe PH (1973) The structures of monoclinic potassium-rich feldspars. Am Mineral 58: 263

Sastre G, Catlow CRA, Corma A (2002) Influence of the intermolecular interactions on the mobility of heptane in the supercages of MCM-22 zeolite. A molecular dynamics study. J Phys Chem (B) 106(5): 956–962

Wartho JA, Kelley SP, Brooker RA, Carroll MR, Villa IM, Lee MR (1999) Direct measurement of Ar diffusion profiles in a gem-duality Madagascar K-feldspar using the ultra-violet laser ablation microprobe (UVLAMP). Earth Planet Sci Lett 170 (1–2): 141–153

Winter JK, Okamura FP, Ghose S (1979) A high-temperature structural study of high albite, monalbite, and the analbite to monalbite phase transition. Am Miner 64: 409–423

Yund RA (1983) Diffusion in feldspars. In: Feldspar Mineralogy. Reviews in Mineralogy vol 2 Mineralogical Society, of America, Washington.DC, pp 203–222